Biofouling film development and its effects on energy losses: a laboratory study

Authors: William G. Characklis, James D. Bryers. Michael G. Trulear, and Nick Zelver

This is a postprint of a book chapter that originally appeared in Condenser Biofouling Control in 1980.

Characklis, W.G., J.D. Bryers, M.G. Trulear, and N. Zelver, "Biofouling Film Development and Its Effects on Energy Losses: A Laboratory Study," in J.F. Garey, et al. (eds.), Condenser Biofouling Control, Ann Arbor Science Publishers, Inc., Ann Arbor, MI, 1980, pp. 49-76.

SECTION II
Mechanisms of Biofouling

CHAPTER 5

BIOFOULING FILM DEVELOPMENT AND ITS EFFECTS ON ENERGY LOSSES: A LABORATORY STUDY

W. G. Characklis, J. D. Bryers, M. G. Trulear and Nick Zelver
George R. Brown School of Engineering
Rice University
Houston, Texas 77001

INTRODUCTION

The term "fouling" refers to the formation of inorganic and/or organic deposits on surfaces. In cooling systems, these deposits form on condenser tube walls, increasing fluid frictional resistance, accelerating corrosion and impairing heat transfer. Four types of fouling, alone or in combinations, may occur:

1. crystalline fouling caused by precipitation of $CaCO_3$, $CaSO_4$ or silicates;
2. corrosion fouling resulting from formation of insulating layers of metal oxides on the tubes;
3. fouling due to adherence of particulate matter on tube surfaces; and
4. biological fouling resulting from development of an organic film consisting of microbial organisms and their products, primarily extracellular polymers.

This investigation was restricted to biological fouling processes.

The Problem

The most common method for controlling fouling biofilm development and maintaining condenser performance is periodic chlorination. Chlorine, added to the cooling water, either kills the microorganism or hydrolyzes the extracellular polymers which hold the biofilm together. The chlorine dosage and application schedule is typically determined by: (1) observation of condenser performance as indicated by plant steam back-pressure, or (2) operator experience.

Recently, concern over residual toxicity from hypochlorous acid or its reaction products has resulted in federal regulations which limit the allowable concentrations of free available chlorine in cooling water discharges. At the present, there is no sound basis for assessing the impact of the regulations. This investigation stems from the apparent need for a more fundamental understanding of fouling biofilm development and fouling biofilm destruction so that the impact of these new regulations on power plant operations can be evaluated.

Laboratory experiments and a limited number of field tests were conducted with two reactor configurations:

1. a tubular reactor; and
2. an annular reactor consisting of a stationary outer cylinder and a rotating inner cylinder.

The tubular reactor geometry and its turbulent flow regime are identical to those existing in power plant condensers. The annular reactor was tested as a biofouling monitor because its response (in terms of fluid frictional resistance) is very sensitive to fouling, and the reactor system is easy to operate and maintain. The annular reactor also has potential for use in a sidestream from the cooling water supply at a power plant to continuously monitor biofouling for control of the addition of oxidant. Biofouling in the experimental reactors was measured by observing changes in the following parameters:

1. biofilm thickness;
2. attached biomass;
3. fluid frictional resistance; and
4. heat transfer resistance.

The project goals included the following:

1. to develop a better understanding of fouling biofilm development, with particular emphasis on the effects of fluid flowrate, bulk water temperature, wall surface temperature and limiting nutrient concentration;
2. to determine the effectiveness of fouling biofilm destruction by chemical oxidants, primarily chlorine; and
3. to develop a practical, reliable and sufficiently sensitive device for monitoring biofouling and for effectively operating and controlling biofouling destruction processes at operating power plants.

Processes Contributing to Fouling Biofilm Development

Microbial fouling is the result of physical transport and biological growth rate processes. The following processes contribute to overall biofouling accumulation:

- organic adsorption at the wetted surface
- transport of microbial particles to the surface
- microorganism attachment to the surface
- growth of attached microorganisms
- reentrainment of biofilm by fluid shear stress

Organic Adsorption

Microorganisms select their habitats on the basis of many factors [1,2], including the nature of the wetted surface (material of construction and surface roughness).

Figure 1 illustrates an initially "clean" surface exposed to turbulent flow of a fluid containing dispersed microorganisms, nutrients and orgenic macromolecules. Adsorption of an organic monolayer occurs within minutes of exposure as shown in Figure 2. Investigations have shown that materials with diverse surface properties (e.g., wettability, surface tension, electrophoretic mobility) are rapidly conditioned by adsorbing organics once exposed to natural waters with low organic concentrations [3–8].

Transport of Microbial Particles to the Surface

Figure 3 indicates the physical transport of bacterial particles from the bulk fluid to the surface covered by an organic film. Within a turbulent flow regime, particles suspended within the fluid are transported to the solid surface by only two mechanisms: molecular diffusion and turbulent eddy transport. Theory indicates that the flux of particles to the surface increases with increasing fluid velocity and particle concentration. However, particle flux

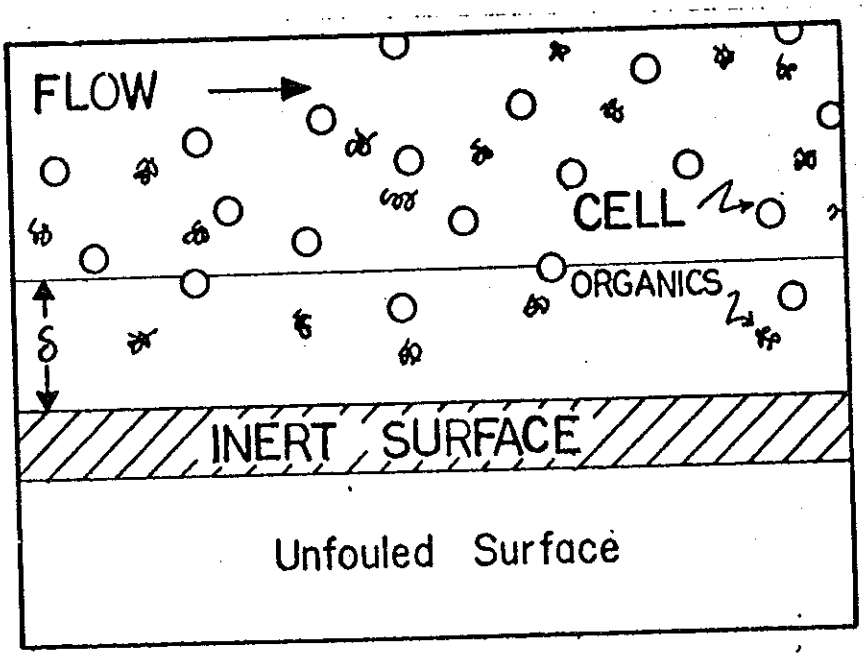

Figure 1. Initially clean surface exposed to a turbulent flow of fluid containing microorganisms and associated material.

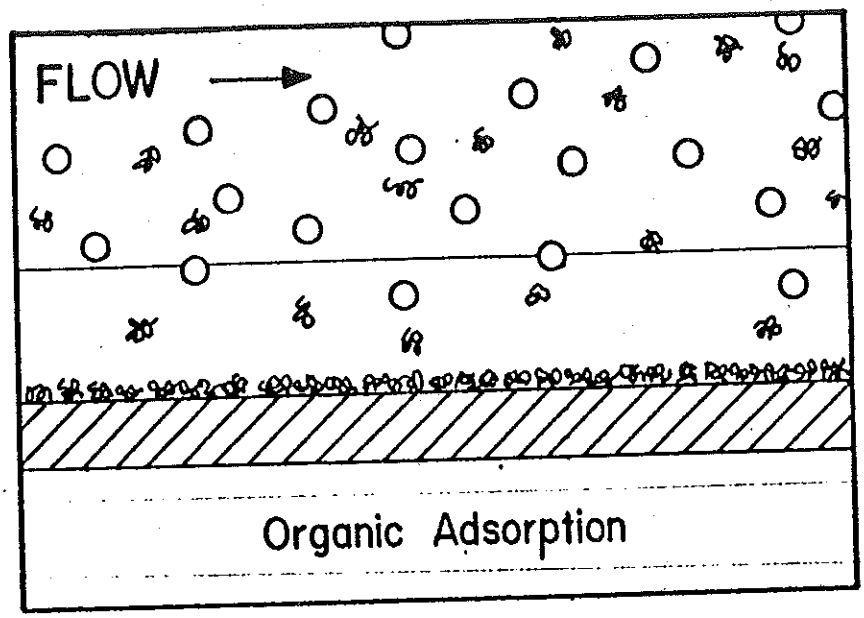

Figure 2. Adsorption of organic material from the bulk fluid.

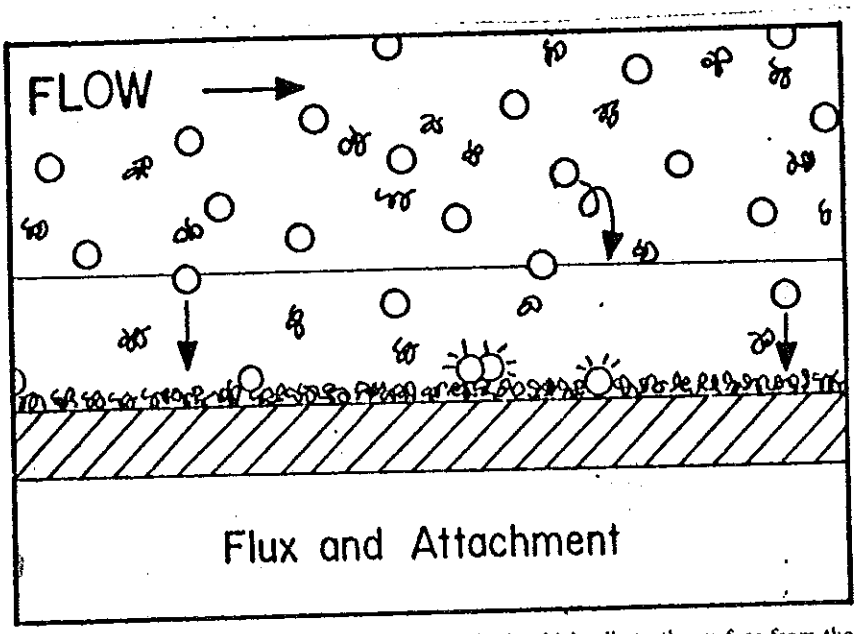

Figure 3. Flux to the surface and attachment of microbial cells to the surface from the bulk fluid.

also depends strongly on the physical properties of the particles (e.g., size, shape, density) [9,10].

Microorganism Attachment to the Surface

Research suggests the existence of a two-stage attachment process: reversible adhesion followed by an irreversible attachment. Reversible attachment refers to an initially weak adhesion of a bacterium to a surface. Organisms still exhibit Brownian motion and are readily removed by mild rinsing. Conversely, irreversible attachment is a permanent cohabitation with the surface, usually aided by the production of cellular exopolymers. Irreversibly attached bacteria can only be removed by severe methods.

Many of the microbial cell attachment studies were conducted at very low fluid shear rates or under quiescent conditions. Rates of accumulation determined from these studies are very likely mass transfer-limited and not necessarily applicable to condenser biofouling where fluid shear rates are quite high (equivalent to average fluid velocities of 6 ft/sec in a 0.75-in. i.d. tube).

Growth of Attached Microorganisms

Attached and dispersed microorganisms assimilate nutrients, synthesize new biomass and produce extracellular polymers. Biomass production is the result of cellular reproduction and exopolysaccharide production, as shown in Figure 4.

Biofilm growth has been described by a wide variety of rate expression whose rate constants are functions of pH, temperature, limiting nutrient concentration, nutrient type, terminal electron acceptor and organism concentration.

Postulated rate expressions for nutrient depletion by a fixed biofilm are numerous [11–16], but all agree that nutrient depletion rates are first-order in biofilm mass and that diffusion rates in the biofilm can often control the overall removal rate of nutrients.

Reentrainment of Biofilm by Fluid Shear

At any point in the development of a biofilm, portions of biofilm peel away from the inert surface and are reentrained in the fluid flow (Figure 5). Reentrainment is a continuous process of biofilm removal and depends highly on hydrodynamic conditions [15]. Sloughing, on the other hand, appears to be a random, massive removal of biofilm attributed to oxygen/nutrient depletion deep within biofilms. Sloughing is more frequently witnessed with thicker, denser films, especially in laminar flow. More work is needed to quantify either effect.

In summary, biofouling is the result of the simultaneous occurrence of all these rate processes (Figure 6). However, at specific times in the overall biofilm development, certain processes may contribute more significantly than others.

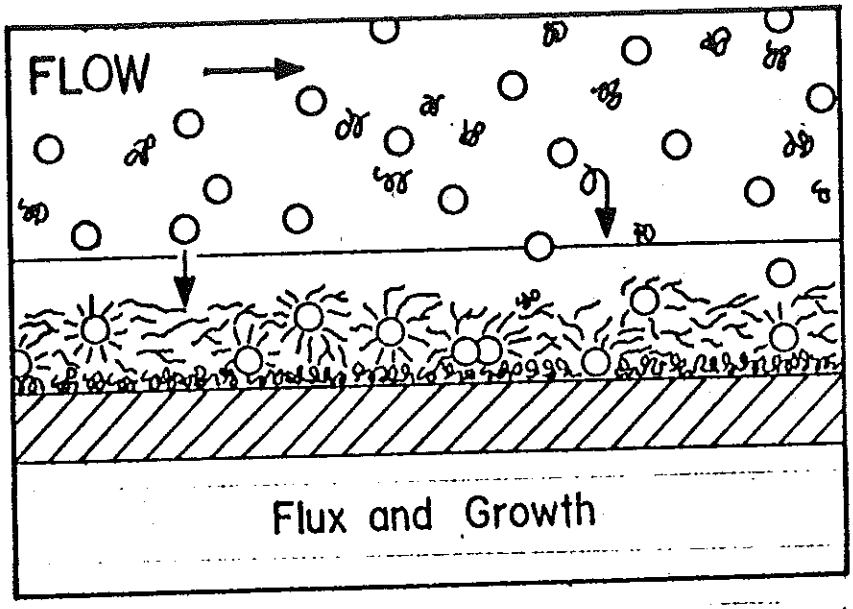

Figure 4. Continued flux of microbial cells to the surface with simultaneous growth processes occurring.

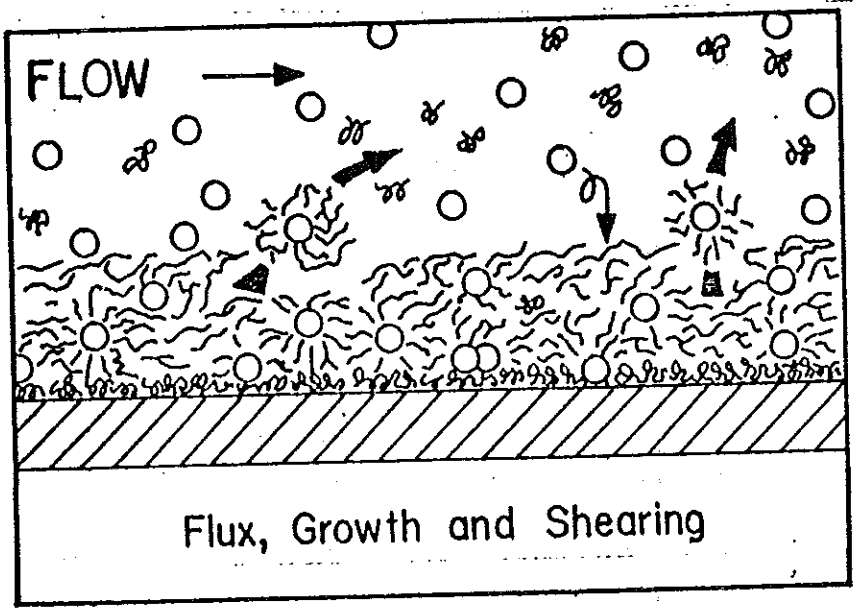

Figure 5. Continued flux of microbial cells to the surface and simultaneous growth processes opposed by reentrainment of biomass due to fluid shear.

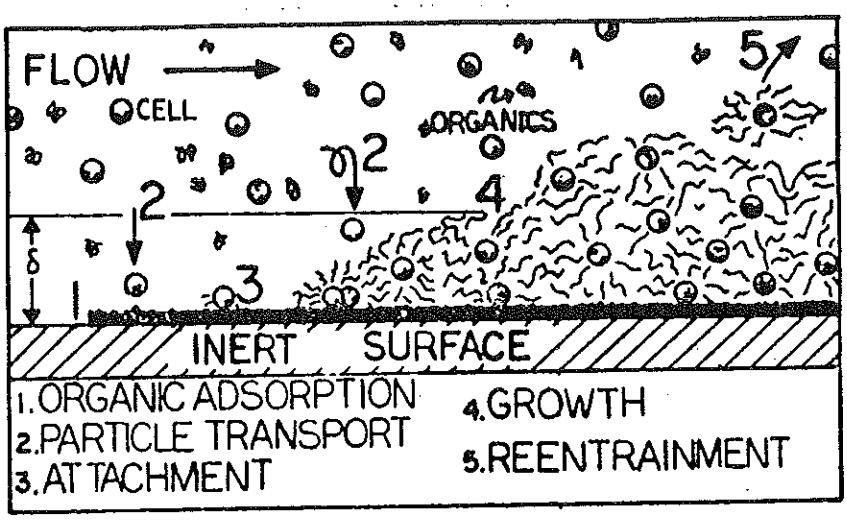

Figure 6. Summary diagram of hypothesized biofouling processes.

EXPERIMENTAL METHODS

The experimental methods used in this laboratory study were chosen to simulate the fundamental processes of biofilm development and destruction occurring in a small portion of a power plant condenser. The laboratory environment was necessary to maintain good control of the variables of interest, i.e., flowrate, temperature and water quality. Nutrients, glucose and, in some cases, a synthetic growth medium, were added to provide the necessary mineral, energy and carbon requirements for microbial growth. The feedwater to the various experimental reactors was tapwater which had been treated to remove residual suspended solids and chlorine.

Experiments which simulated the growth to plateau phases (Figure 7) were initiated by inoculating with a mixed population of microorganisms and operating the reactors in a batch mode (as opposed to continuous flow) until some surface colonization occurred. This technique minimizes the induction period (Figure 7), which can last for weeks under some of the conditions tested. The recycle reactor in experiments simulating the induction period is fed from a chemostat (i.e., a microbial cell propagator).

There are always risks in applying results from a laboratory simulation to a problem in a field. Some such limitations for this study are presented in the Results and Discussion section.

Experimental Apparatus

Two reactor geometries were used in this reasearch to study biofilm development and destruction:

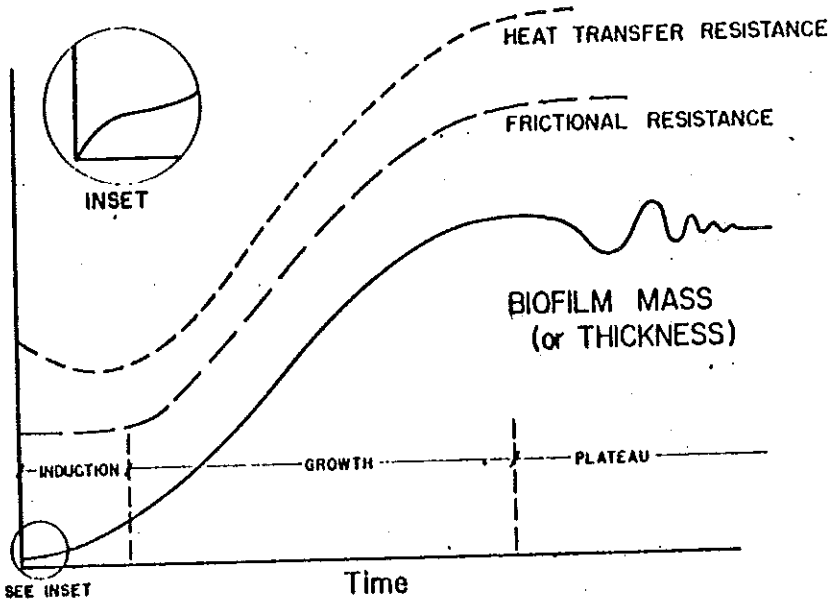

Figure 7. Typical progression of biomass accumulation and resulting energy losses in experimental systems.

1. The circular tube was used because it is the prevalent geometry in power plant condensers.
2. The sensitivity of the rotating annular reactor was tested because it could provide more practical, reliable means of monitoring biofouling in the field, since it requires little maintenance or support equipment. This chapter will not discuss results from the annular reactor.

Biofilm development was measured in two ways: (1) attached biomass, and (2) biofilm thickness. During the induction phase biofilm development was measured with chemical oxygen demand (COD) analysis because of its superior sensitivity.

Indirectly, biofouling was observed by measuring: (1) fluid frictional resistance, and (2) heat transfer resistance.

Tubular Fouling Reactors

Tubular fouling reactors are chemostats (continuously stirred tank reactors) with internal recycle as indicated in Figure 8. Advantages of this configuration for laboratory experimentation include the following:

1. At high recycle rates ($F_r \gg F$), the reactor contents are completely mixed and no concentration gradients exist. This simplifies mathematical descriptions and sampling. It also provides a relatively uniform biofilm in the recycle section while allowing simple control of pH and temperature. From a practical standpoint, this system minimized the consumption of water and microbial nutrient medium.

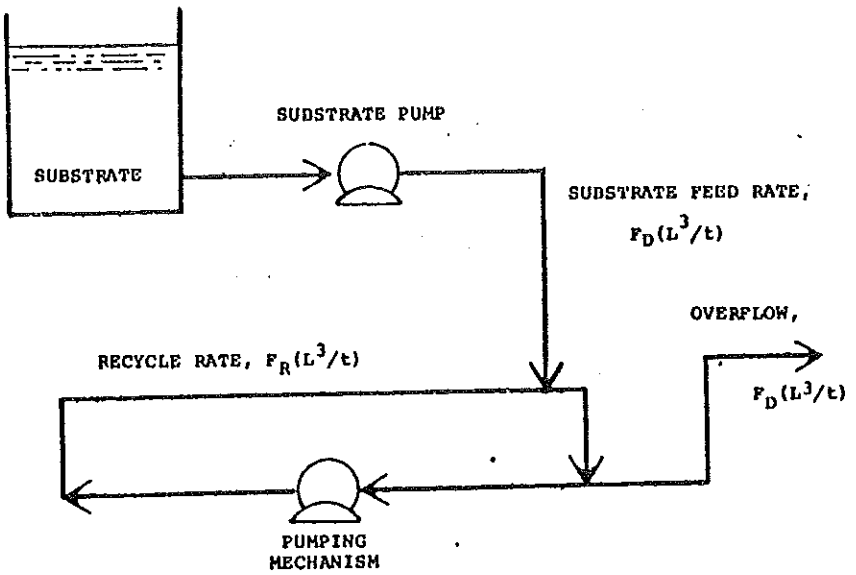

Figure 8. Schematic diagram of tubular reactor system with internal recycle.

2. A short mean residence time can be maintained, which minimizes biomass activity in the bulk fluid and restricts microbial activity to the reactor surfaces.
3. Fluid shear stress at the wall in the recycle loop is independent of mean residence time in the reactor system.

The results from three tubular reactors are discussed in this paper.

Tubular fouling reactor 1 (TFR1) was used to determine the effect of fluid shear rate at the wall, bulk water temperature and limiting substrate concentration on biofilm development as determined by attached biomass, biofilm thickness and fluid frictional resistance. Tubular fouling reactor 3 (TFR3) was an improved version of TFR1 (Figure 9).

Tubular fouling reactor 4 (TFR4) was used to determine biofilm thermal conductivity. Biofilm thickness, fluid frictional resistance and heat transfer resistance were measured by TFR4 experiments. Heat transfer resistance was measured in a test heat exchanger (THE) which was an integral part of the recycle reactor.

Tubular fouling reactor 5 (TFR5) (Figure 10) was used for studying primary biofouling development. It consists of a continuous culture reactor (i.e., chemostat CSTR) with internal recycle loops. In this way a constant bulk microbial culture can be maintained at a desired activity while independently simulating a variety of hydrodynamic situations.

Further details concerning methods and experimental protocol can be found elsewhere [15–19].

RESULTS AND DISCUSSION

The process of biofilm development on a surface exposed to a turbulent flow is adequately described by a sigmoid-shaped curve. The progression of biofilm development can be conveniently divided into three phases:

1. induction phase—the initial development period during which the biofilm accumulation increases but fluid frictional resistance remains constant;
2. growth phase—the period of time during which the accumulation increases logarithmically (may include a portion of the induction period); and
3. plateau phase—the period during which deceleration of the accumulation rate is observed and a pseudosteady-state in biofilm accumulation occurs.

The three phases of biofilm development are indicated in Figure 7.

Induction Phase

Primary biofilm formation occurs during the period from "clean" surface conditions to the onset of frictional resistance increase.

Experiments were conducted to ascertain the rate of primary biofilm formation as a function of dispersed biomass concentration X, Reynolds number Re and dispersed organism growth rate μ. The relationship can be described as follows:

$$R_i = dX_A/dt = kf^c(X, Re, \mu, X_A) \quad (1)$$

where X_A = attached biofilm amount/area
R_i = rate of initial biofilm formation

All primary biofilm experiments were conducted in TFR1–5, described in Figure 10.

Results of the primary biofilm formation experiments are illustrated in Figures 11–13. The amount of biofilm attached is reported as the mg COD attached per cm^2. Each figure provides a comparison of results conducted at extremes of each of the three parameters considered. Figure 11 illustrates the effect of average fluid velocity or Reynolds number Re on early biofilm development. For both experiments, dispersed biomass concentration was 12 mg TSS/l and dispersed organism growth rate was 0.28 hr^{-1}. Results indicate biofilm develops faster at higher velocity and suggests that, at higher velocity, the particle flux to the surface is higher. Theory indicates an increase in particle deposition coefficient (and thus, particle flux) with increasing velocity [9].

Figure 12 depicts the effect of dispersed biomass concentration on the rate of initial biofilm accumulation. For both experiments, fluid velocity was 108.0 cm/sec and dispersed organism growth rate was 0.29 hr^{-1}. Increasing the concentration of suspended biomass increases the rate of initial biofilm formation. The flux of particles to the surface is directly proportional to the bulk concentration [9].

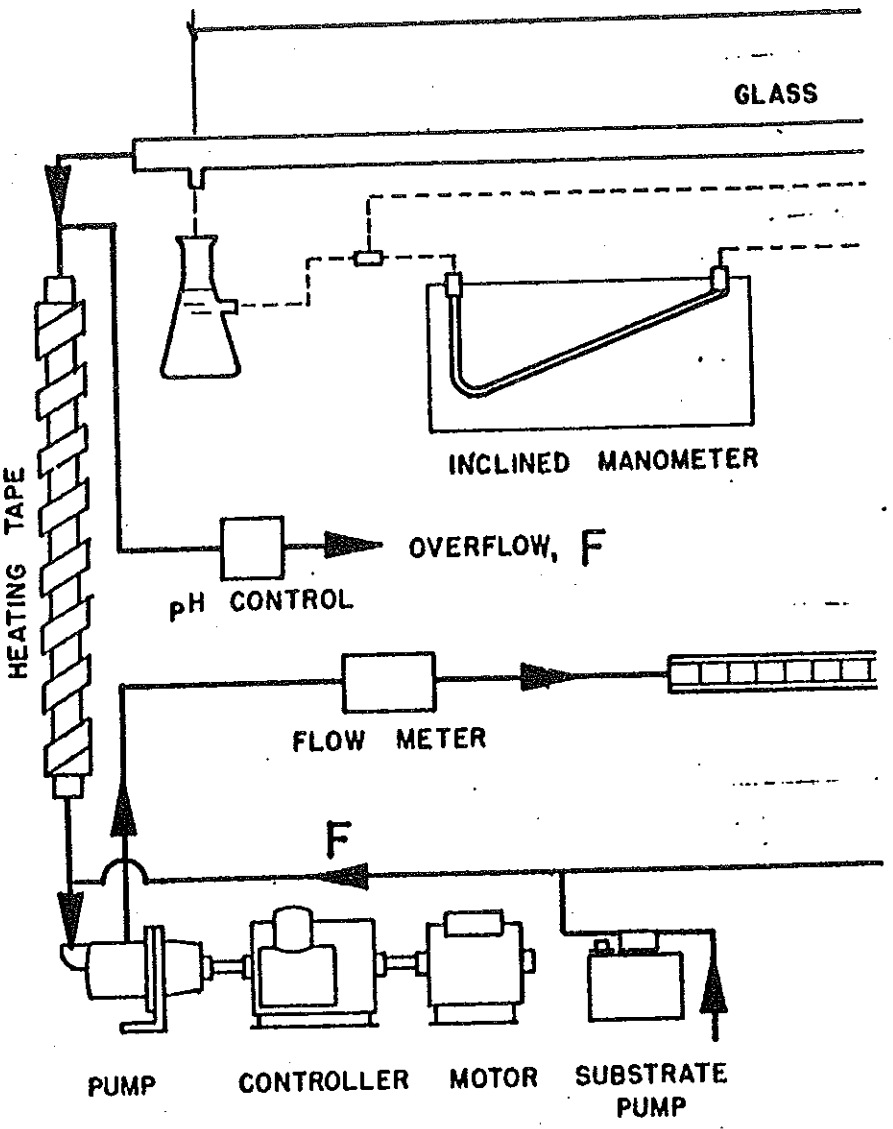

Figure 9. Detailed diagram of [illegible]

Figure 13 clearly exhibits the effect of dispersed biomass growth rate on the rate of primary biofilm formation. For the experiments illustrated, suspended biomass concentration is 15 mg TSS/l and the velocity is 108 cm/sec. As expected, an increase in growth rate of dispersed organism increases the rate of biofilm formation. However, attached biofilm is measured as mg

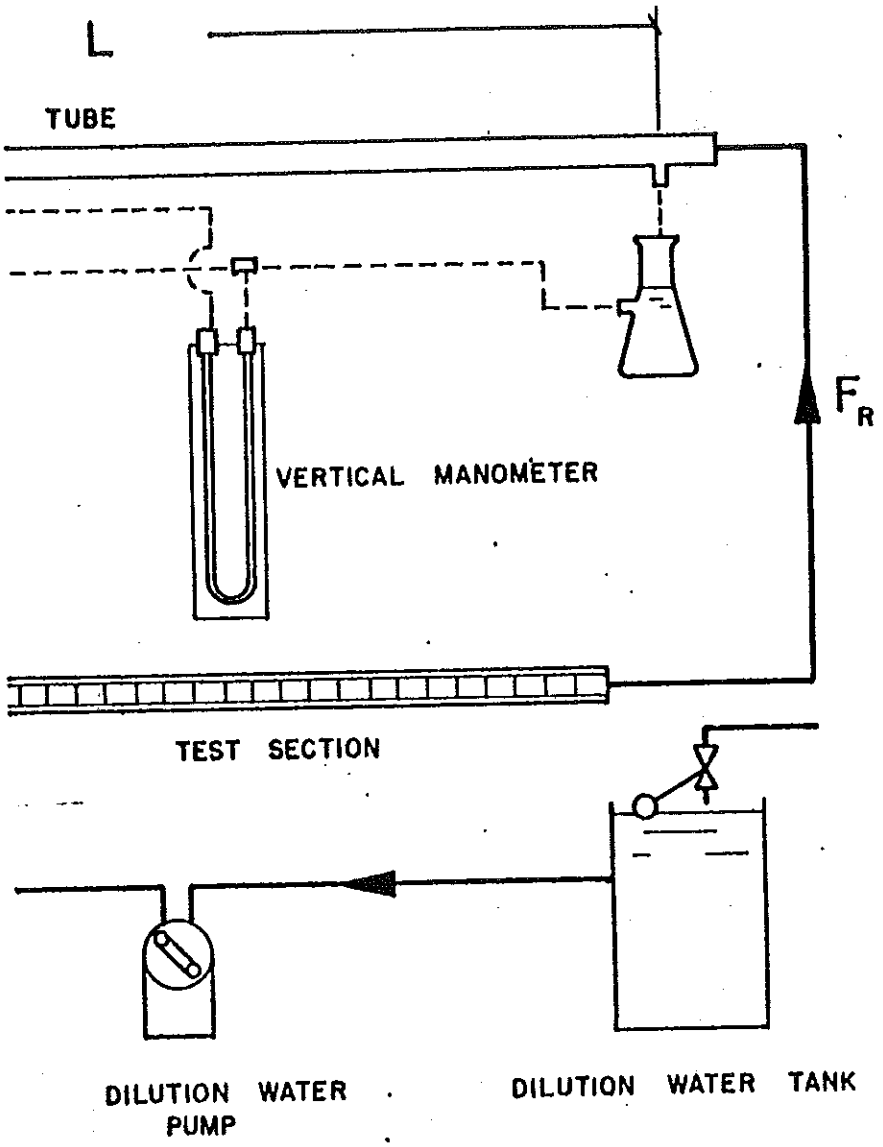

Tubular Fouling Reactor 3 (TFR3).

COD/cm^2, a measure of the amount of oxidizable material attached per area. Results shown in Figure 13 suggest that the increased dispersed growth rate either increases the concentration of attached organisms or increases extracellular polysaccharide production rate. Other results suggest that the latter occurs.

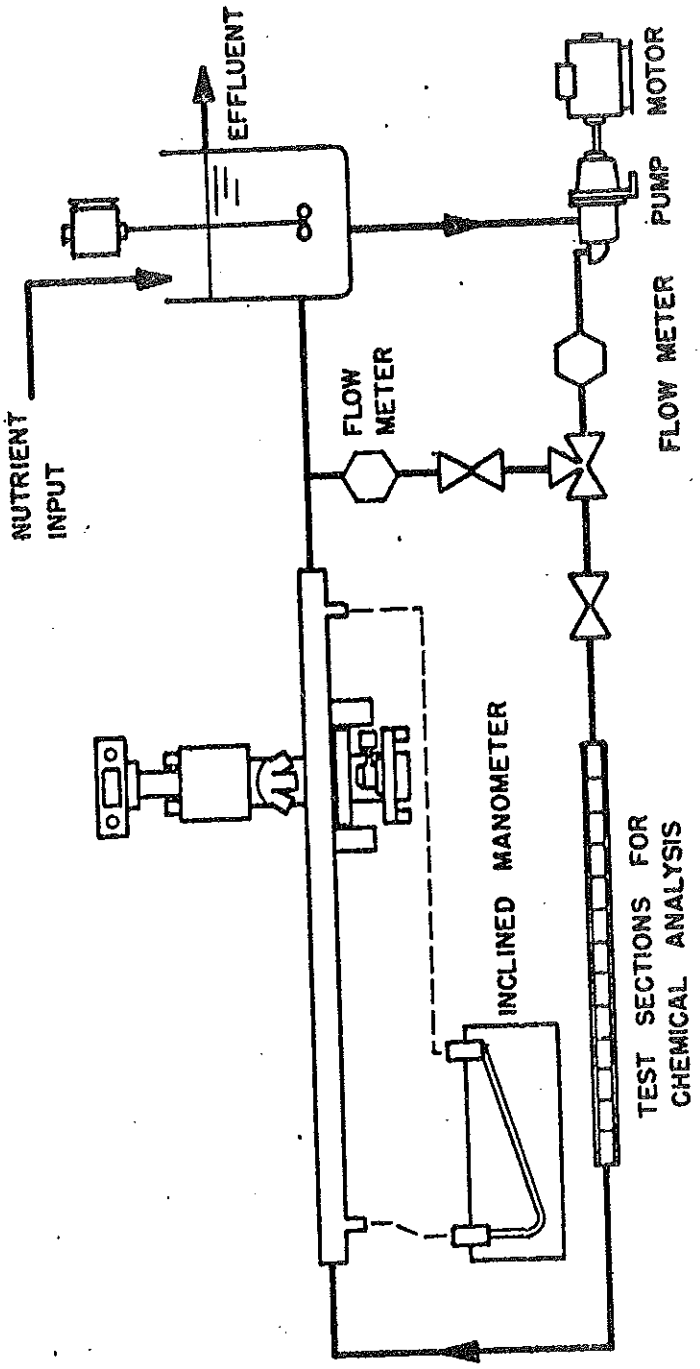

Figure 10. Detailed diagram of Tubular Fouling Reactor 5 (TFR5).

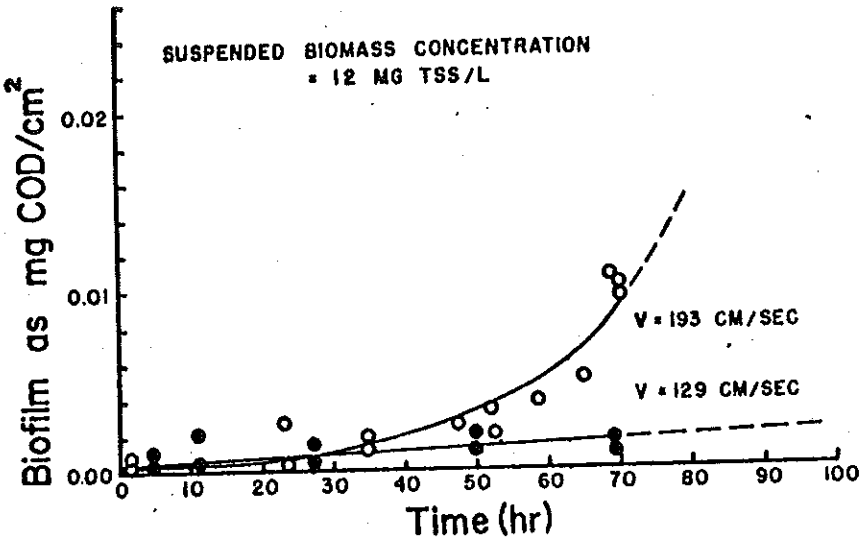

Figure 11. Effect of fluid velocity on biofilm development.

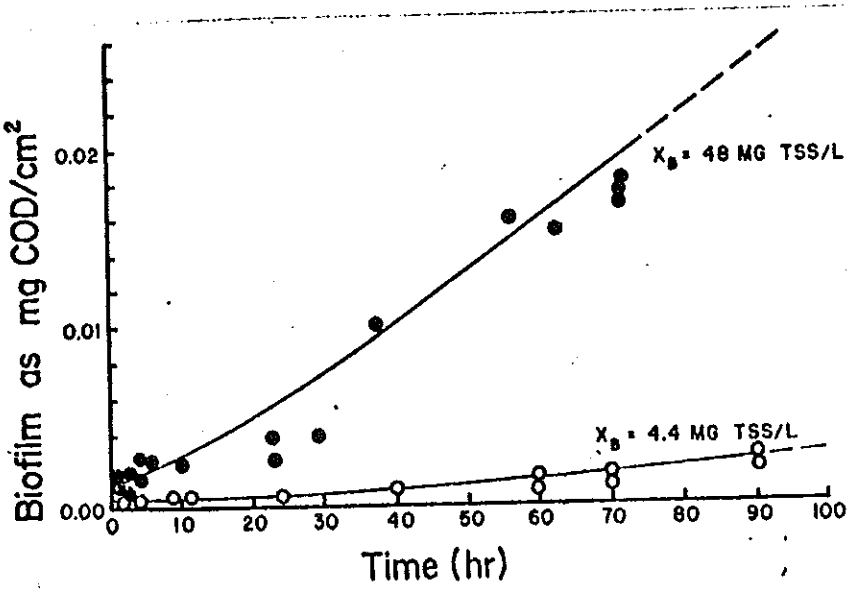

Figure 12. Effect of dispersed biomass concentration on biofilm development.

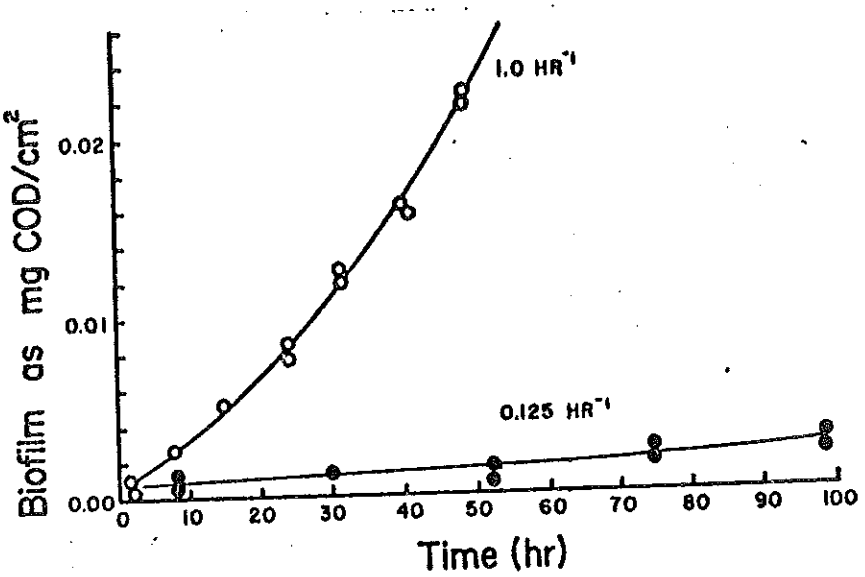

Figure 13. Effect of dispersed microbial growth rate on biofilm development.

Growth and Plateau Phases

The growth phase, a logarithmic growth period, overlaps the induction phase and is followed by the plateau phase. Energy losses are significant during these two phases. The progression of biofilm development for a typical experiment is illustrated in Figure 7. The logistic or sigmoidal curve for biofilm development can be described analytically by:

$$Th = \frac{Th_0 e^{kt}}{1 - (Th_0/Th_{MAX})(1 - e^{kt})} \tag{2}$$

where Th = biofilm thickness (L)
Th_0 = Th at t = 0 (L)
Th_{MAX} = maximum value of Th attained (L)
k = rate constant (t^{-1})

The rate of change of Th can be described by:

$$\frac{d(Th)}{dt} = k(Th) - \frac{k(Th)^2}{Th_{MAX}} \tag{3}$$

The rate constant k describes the logarithmic rate of development which occurs at $Th \ll Th_{MAX}$. The second term accounts for some process opposing development. Regardless of mechanism, k(Th) represents the logarithmic development rate or fouling rate characteristic of the growth phase while Th_{MAX} characterizes the plateau phase.

The logarithmic fouling rate (based on either biofilm thickness or biofilm mass) varies with nutrient loading rate as indicated in Figure 14. The effect of wall shear stress is also indicated. As wall shear stress increases, the second term in Equation 3 becomes more important in controlling biofilm development rate. This suggests that Th_{MAX} decreases with increasing wall shear stress. Figure 15 indicates that, in fact, Th_{MAX} decreases with increasing wall shear stress, especially at high nutrient loading rates.

Effects on Frictional Resistance

Increase in fluid frictional resistance because of biofilm accumulation during experiments in which flowrate is maintained constant causes an increase in pressure drop and power requirements for pumping as shown in Figure 16 for a typical experiment.

Conversely, if pressure drop is held constant, flow capacity is reduced. Figure 17 shows a typical experimental curve where flow capacity was reduced to 42% of the original capacity in a 100-h laboratory experiment.

Frictional resistance can be represented by a dimensionless friction factor given by:

$$f = 2.0 \frac{d}{L} \frac{\Delta P}{\rho_w \bar{v}^2} \tag{4}$$

where f = friction factor (dimensionless)
d = tube diameter (L)
ρ_w = fluid density (M/L^3)
$\bar{v}$ = average fluid velocity (L/t)
ΔP = pressure drop along length L ($M/L/t^2$)
L = length between pressure ports (L)

The change in friction factor with time for a typical experiment is shown in Figure 18. The measured biofilm thickness for the same experiment is also indicated.

The friction factor is related to the Reynolds number and the equivalent sand roughness k_s through the empirical Colebrook-White relation. This equation correlates friction factor to Reynolds number for various "commercially rough" pipes throughout the hydraulically smooth, transition and fully rough regimes. The Colebrook-White equation, solved for the equivalent sand roughness k_s yields:

$$k_s = \frac{d}{2}\left[10^{(0.87 - 0.50 f^{-1/2})} - \frac{18.70}{Re f^{1/2}}\right] \tag{5}$$

where d = tube diameter (L)
$Re = \bar{v}d/\nu$ = Reynolds number (dimensionless)
$\bar{v}$ = mean fluid velocity (L/t)
ν = kinematic viscosity (L^2/t)

This expression can be used to compute an equivalent sand roughness for the biofilm from a measurement of the flowrate and pressure drop.

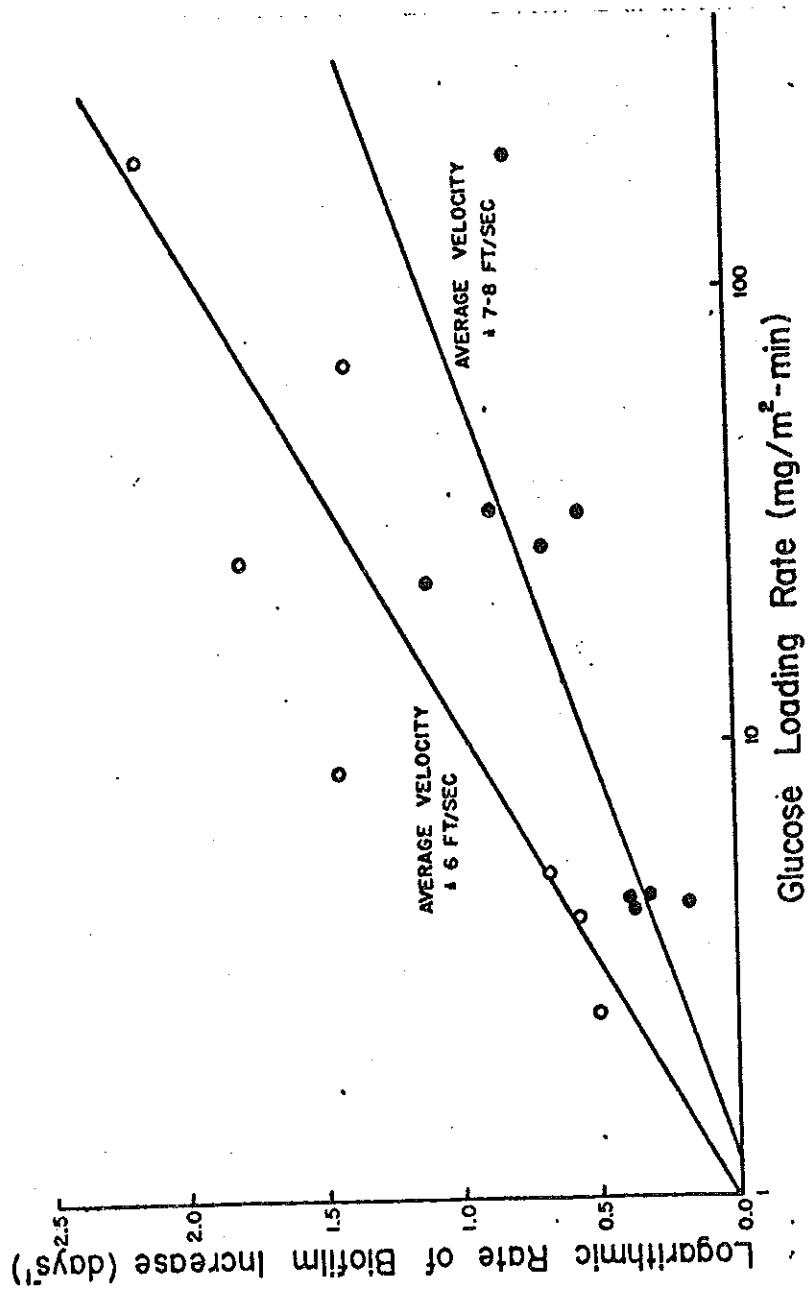

Figure 14. Effect of glucose loading on rate of biofilm development.

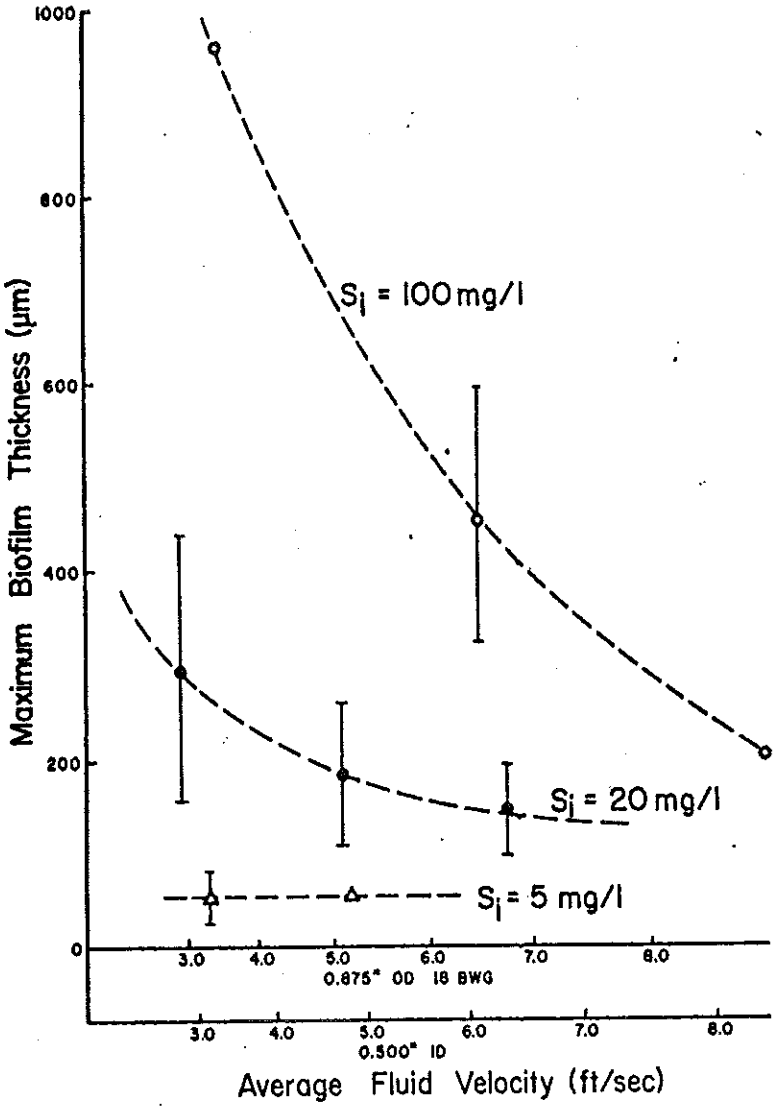

Figure 15. Effect of nutrient loading and fluid shear on maximum biofilm thickness attained.

In all TFR experiments, k_s increases with time; Figure 19 shows the progression of k_s with time for a typical experiment. Figure 20 indicates the dependence of k_s on biofilm thickness for the range of shear stress investigated (6.5–7.9 N/m^2).

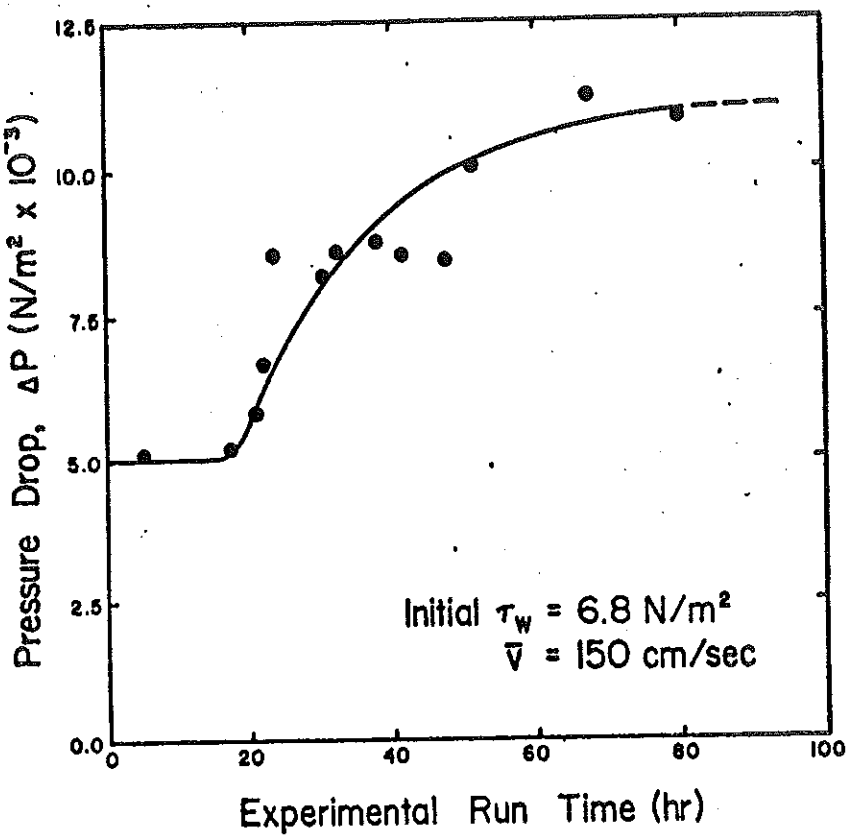

Figure 16. Increase in a pressure drop during a typical experiment in which fluid flow-rate was maintained constant.

Determination of the flow regime (smooth, transitional or fully rough) depends on the magnitude of k_s relative to the size of the viscous sublayer (δ_1):

$$\delta_1 = \frac{10d}{Re}\left(\frac{f}{2}\right)^{-0.5} \tag{6}$$

More specifically, when $k_s < \delta_1$, the pipe is considered hydraulically smooth; when $14\delta_1 > k_s > \delta_1$ the flow is in the transitional regime; when $k_s > 14\delta_1$, the flow is in the fully rough regime [20]. In all experiments, the flow regime, as determined from the above criteria, progressed from hydraulically smooth to transitional or fully rough.

Frictional resistance of biofilms grown under constant pressure drop have

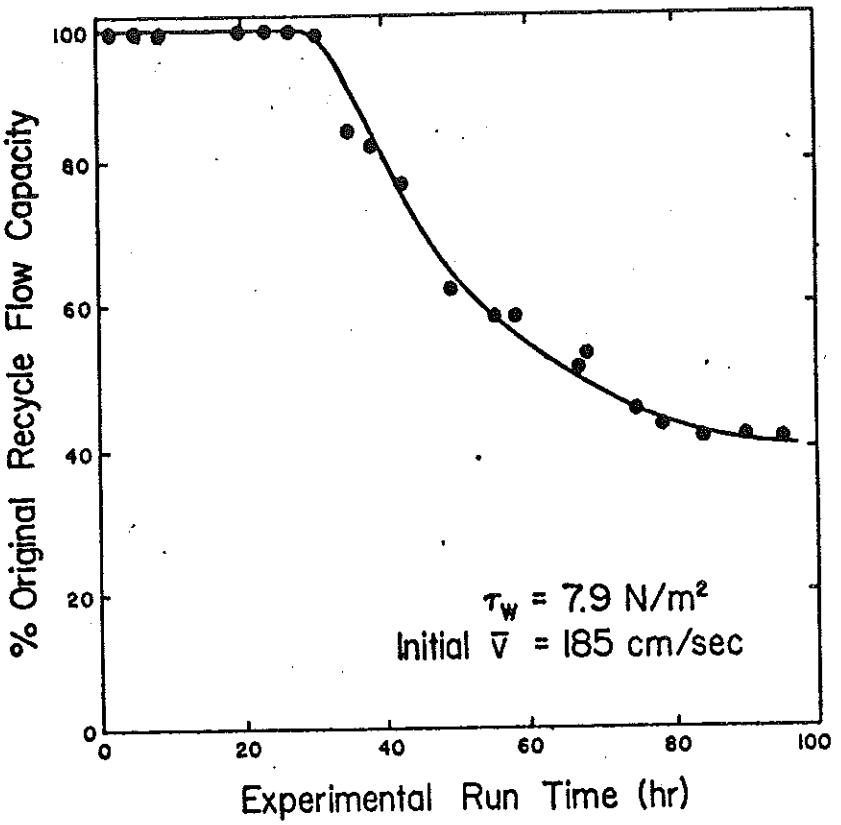

Figure 17. Decrease in fluid flowrate during a typical experiment in which pressure drop was maintained constant.

been compared to the frictional resistance of pipes with a rigid roughness as given by the Colebrook-White equation. The following was observed:

1. Frictional resistance because of biofilm shows a similar dependency on Reynolds number as frictional resistance because of commercially rough pipe surface.
2. Frictional resistance depends on biofilm thickness.
3. Frictional resistance does not increase above the hydraulically smooth pipe value until a critical biofilm thickness is obtained.

The Blasius-Stanton or Moody diagram [21] can be used to compare frictional resistance due to biofilm with frictional resistance of rigid rough surfaces. The Blasius-Stanton diagram is a plot of friction factor vs Reynolds number for a series of pipes with different equivalent sand roughness; the

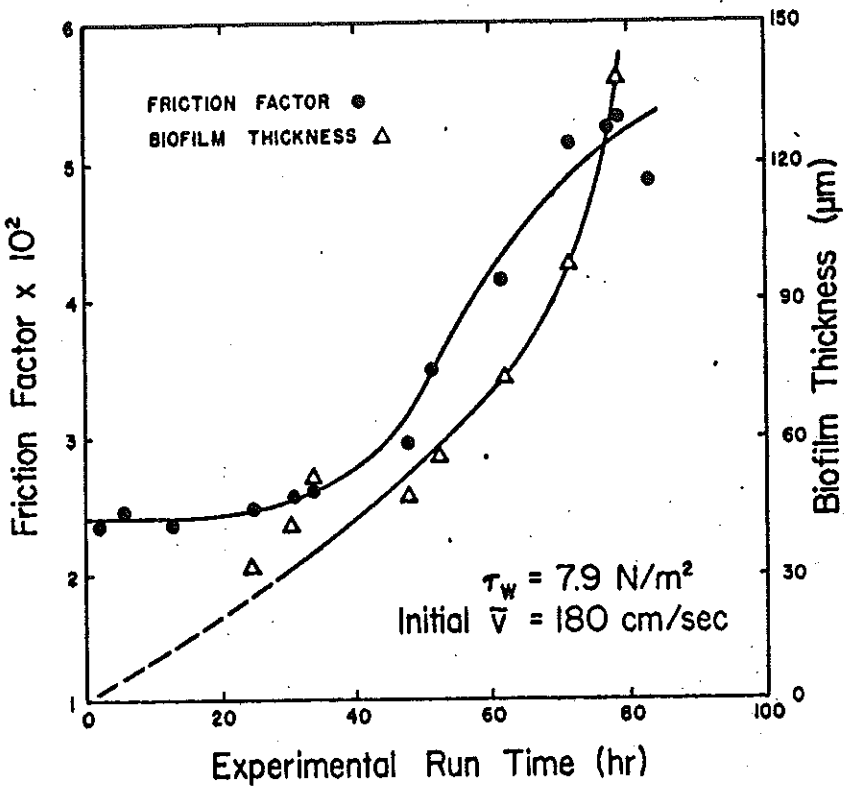

Figure 18. Change in friction factor and biofilm thickness during a typical experiment.

friction factor in a pipe with a rigid rough surface depends on both the relative roughness and the Reynolds number.

The relationship between friction factor and Reynolds number for the fouled TFR3 system is presented in Figure 21. The friction factors and Reynolds numbers presented have not been corrected for the pipe constriction resulting from the biofilm. This figure shows the dependency of friction factor on Reynolds number is the same as for a tube with a rigid rough surface between the range of Reynolds numbers investigated (5000–48,000). This data was obtained by reducing, in steps, the shear stress from its initial value in a given experiment and calculating friction factor and Reynolds number at each step. The shear stress was reduced from the initial condition to minimize sloughing of biofilm during an experiment.

Figure 22 indicates the relationship between friction factor and Reynolds number for an experiment at different stages of biofilm development; friction factor increases with biofilm thickness. The relationship between biofilm

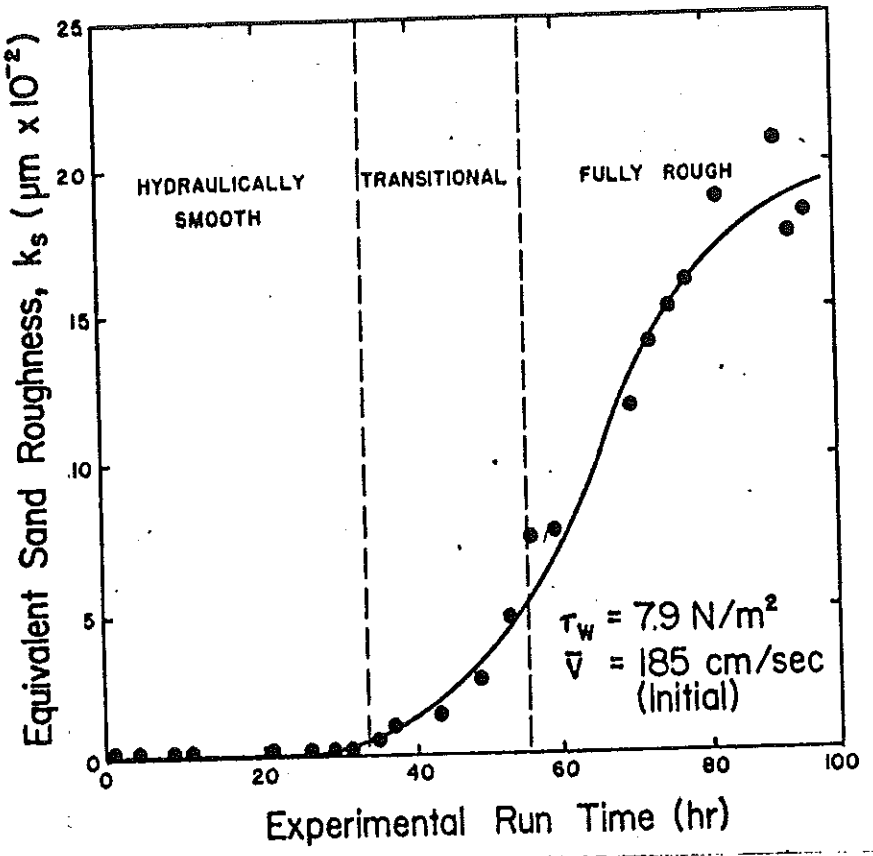

Figure 19. Change in equivalent sand roughness during a typical experiment.

thickness and friction factor for all experiments at a wall shear stress from 6.5–7.9 N/m^2 is shown in Figure 23. Friction factor is dependent on film thickness after attainment of a critical thickness (TH_{crit}) approximately equal to the thickness of the viscous sublayer.

The critical film thickness corresponds to the stage of biofilm development at which surface irregularities protrude through the viscous sublayer. Until this stage, the biofilm lies completely within the viscous sublayer ($k_s < \delta_1$) and friction factor does not increase (the tube is hydraulically smooth). For a wall shear stress of 6.5–7.9 N/m^2, the viscous sublayer is approximately equal to 40 μm; this compares well with the observed TH_{crit} of 30–35 μm for the same wall shear stress range.

Although the frictional resistance effects of biofilm can be described adequately by formulae suitable for rigid rough surfaces, the conclusion

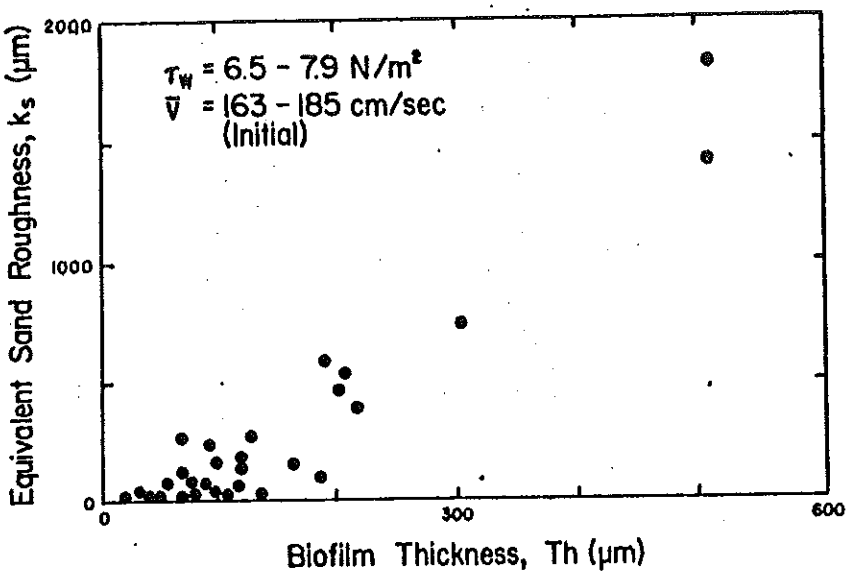

Figure 20. Variation in equivalent sand roughness with changing biofilm thickness.

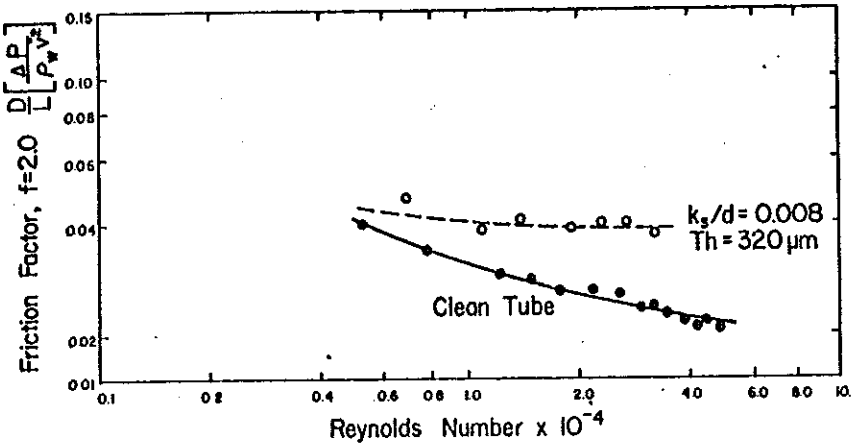

Figure 21. Relationship of friction factor and Reynolds number for the clean tube and for a fouled tube.

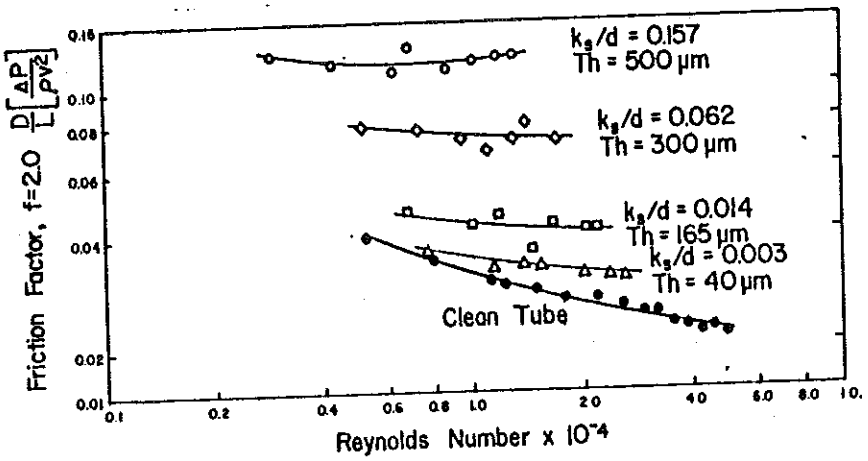

Figure 22. Relationship of friction factor and Reynolds number as biofilm develops in a particular experiment.

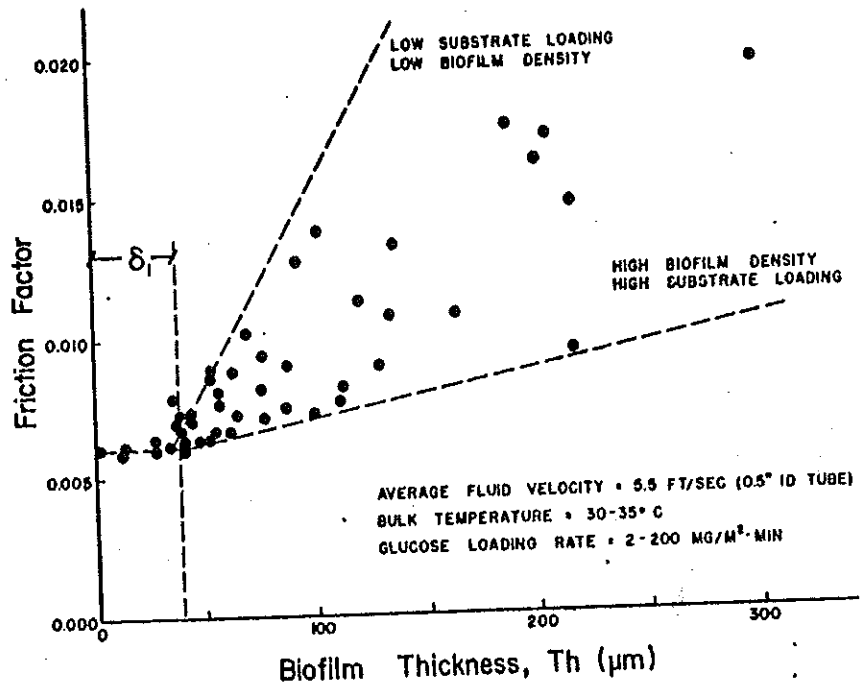

Figure 23. The effect of biofilm thickness on friction factor in a circular tube.

should not be drawn that indeed the biofilm presents a rigid rough surface to the flow. Such a notion is an oversimplification and cannot account for all experimental observations [22].

Effects on Heat Transfer Resistance

Biofilm development and resulting fluid frictional resistance have been discussed, and both influence heat transfer. Changes in heat transfer resistance arise from the combined effects of increased biofilm thickness (conductive heat transfer) and increased frictional resistance (convective heat transfer).

Conductive heat transfer can be related to biofilm thickness and its effective thermal conductivity. Experimental biofilm thermal conductivity determinations indicate no significant difference from that of water at the same temperature (Table I). This is not surprising, since biofilm is approximately 98–99% water.

Convective heat transfer results from fluid mixing or motion, and can be related to momentum transfer or frictional resistance. Colburn [23] correlated convective heat transfer in tubes to friction factor and properties of the fluid. The Colburn relationship is only useful when the biofilm is thicker than the viscous sublayer.

Overall heat transfer resistance due to biofouling film development can then be calculated if the following are known:

1. biofilm thickness and thermal conductivity;
2. frictional resistance; and
3. wall temperature and bulk temperature.

Figure 24 describes a typical experiment in TFR4 and illustrates the relative effects of conductive and convective heat transfer resistance on overall heat transfer resistance.

Table I. Thermal Conductivity of Biofilms

Experiment	Input Glucose Conc (mg/l)	Biofilm Thermal Conductivity (W/m-°C)	Bulk Temperature (°C)
1	100	0.70 ± 0.40 (3)	31.89 ± 0.49
2	10	0.71 ± 0.10 (3)	31.50 ± 0.03
6	10	0.68 ± 0.22 (5)	28.30 ± 0.03
7	25	0.52 ± 0.21 (3)	26.70 ± 0.03
8	10	0.70 ± 0.38 (5)	26.70 ± 0.03
9	10	0.58 ± 0.14 (5)	28.30 ± 0.03
	Grand mean	0.65 ± 0.24 (24)	
	Water	0.61	26.7
	Water	0.62	32.2

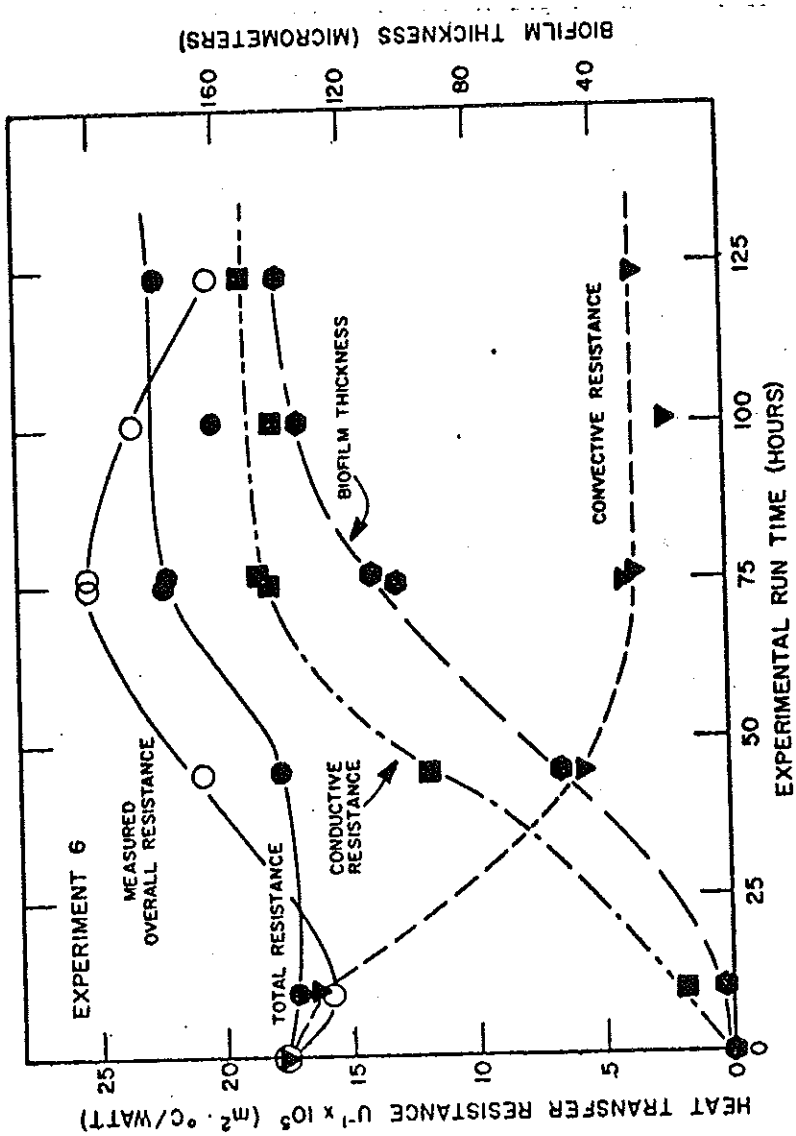

Figure 24. Heat transfer resistance changes with time as a result of biofilm development.

SUMMARY

Current research has provided some insight into the overall biofouling problem.

1. Biofouling film development is the combination of several physical transport and biological rate processes.
2. Rate of biofouling in the induction phase increases with increasing dispersed organism concentration, fluid flow velocity and dispersed organism growth rate.
3. Rate of biofouling in the growth phase increases with increasing nutrient loading rate and decreasing fluid flow velocity.
4. The maximum biofilm thickness attained increases with increasing nutrient loading and decreasing fluid flow velocity.
5. Beyond a "critical" thickness, biofilm accumulation may create large increases in both frictional and heat transfer resistances. The "critical" biofilm thickness, observed experimentally, compares favorably with the viscous sublayer thickness calculated for flow in the clean tube.
6. Increased frictional resistance resulting from biofilm development can be attributed to several biofilm characteristics including its viscoelasticity, filamentous morphology and/or rippling surface morphology. Regardless of mechanism, the increase in friction factor can be described by traditional "equivalent sand roughness" concepts.
7. Changes in overall heat transfer resistance arise from the effect of biofilm development on both conductive and convective heat transfer.

ACKNOWLEDGMENTS

The authors gratefully acknowledge the Electric Power Research Institute (RP902-1), the National Science Foundation (ENG 74-11957 and ENG 77-26934) and the Amoco Fellowship Foundation for partial financial support; Drs. B. F. Picologlou and L. V. McIntire for significant contributions to the experimental program; Maurine Lee and Linda Graetz for manuscript preparation; and Duane Marks for graphics preparation.

REFERENCES

1. Brock, T. D. *Principles of Microbial Ecology* (Englewood Cliffs, NJ: Prentice Hall, 1966).
2. Meadows, P. S. "The Attachment of Bacteria to Solid Surfaces," *Arch. Mikrobial* 75:671 (19xx).
3. Baier, R. E., E. G. Shafin and W. A. Zisman. "Adhesion: Mechanisms that Assist or Impede it," *Science* 162(2):1360 (1968).
4. Baier, R. E. "Influence of the Initial Surface Condition of Materials on Bioadhesion," Proc. 3rd Int. Cong. on Marine Corrosion and Biofouling, Gaithersburg, MD, 1972.

5. Baier, R. E. "Applied Chemistry at Protein Interfaces," *Adv. Chem. Series*, #145, American Chemical Society (1973), p. 1.
6. Baier, R. E., and V. A. Depalma. "Microfouling of Metallic and Coated Metallic Flow Surfaces in Model Heat Exchanger Cells," (Buffalo, NY: Calspan Corp., 1977).
7. Loeb, G., and R. Neihof. "Molecular Fouling of Surfaces in Seawater," Proc. 3rd Int. Cong. on Marine Corrosion and Biofouling, Gaithersburg, MD, 1972.
8. Loeb, G., and R. Neihof. "Marine Conditioning Films," *Adv. Chem. Series*, #145, American Chemical Society (1973), p. 319.
9. Beal, S. K. "Deposition of Particles in Turbulent Flow on Channel or Pipe Walls," *Nuc. Sci. Eng.* 40:1–11 (1970).
10. Friedlander, S. K., and H. F. Johnstone. "Deposition of Suspended Particles from Turbulent Gas Streams," *I. & E. C.* 49(2):1151–1156 (1957).
11. Atkinson, B., and M. E. Abdel Rahman Ali. "Wetted Area, Slime Thickness, and Liquid Phase Mass Transfer in Packed Bed Biological Film Reactors," *Trans. Inst. Chem. Eng.* 54:239–250.
12. Harremoes, P. "Half-Order Reactions in Biofilm Kinetics," *Vatten* 2: 122–143.
13. Kornegay, B. H. "Characteristics and Kinetics of Biological Fixed Film Reactors," PhD Dissertation, Clemson University, Clemson, SC, 1967.
14. LaMotta, E. J. "Evaluation of Diffusional Resistances in Substrate Utilization by Biological Films," PhD Dissertation, University of North Carolina at Chapel Hill, 1974.
15. Trulear, M., and W. G. Characklis. "Dynamics of Biofilm Processes," *Proceedings 34th Annual Industrial Wastewater Treatment Conference, Purdue University* (Ann Arbor, MI: Ann Arbor Science Publishers, Inc., 1979).
16. Zelver, N. "Biofilm Development and Associated Energy Losses in Water Conduits," MS Thesis, Rice University, Houston, TX, 1979.
17. Bryers, J. D., and W. G. Characklis. "Measurement of Primary Biofilm Formation," Chapter 10, this volume.
18. Characklis, W. G. "Biofilm Development and Destruction," Final Report, Electric Power Research Institute RP 902-1, Palo Alto, CA (1979).
19. Nimmons, M. J. "Biofilm Effects on Heat Transfer Resistances within a Turbulent Flow System," MS Thesis, Rice University, Houston, TX, 1979.
20. Schlichting, H. *Boundary-Layer Theory*, 6th ed. (New York: McGraw-Hill Book Co., 1968).
21. Moody, L. F. "Friction Factor Dependency on Reynold's Number and Pipe Roughness," *Trans. ASME* 66:671 (1944).
22. Picologlou, B., N. Zelver and W. C. Characklis. "Influence of Biofilms on Hydraulic Deterioration in Circular Tubes," *J. Hydraul. Div., ASCE* (submitted).
23. Colburn, A. P. "Correlation of Momentum and Energy Transfer," *Trans. Am. Inst. Chem. Eng.* 29:174–210 (1933).